Effect of Welding on The Corrosion Behaviour of a Highly Alloyed Austenitic Stainless Steel UNS N06027 in Polluted Phosphoric Acid Media

S.Bakour[1], A.Guenbour[1,*], A. Bellaouchou[1], C. Escrivà-Cerdán[2], R. Sánchez-Tovar[2], R. Leiva-García[2], J.García-Antón[2,*]

[1] Laboratory Corrosion-Electrochimie, Faculty of Sciences, University Mohammed V-Agdal, BP 1014, Rabat (MORROCO).
[2] Ingeniería electroquímica y Corrosión. Departamento de Ingenieria Quimica y Nuclear, E.E.S.I. Industriales, Universitat Politècnica de València, P.O. Box 221012, E-46071 Valencia, Spain.
[*]E-mail: guenbour@fsr.ac.ma; jgarciaa@iqn.upv.es

The objective of this work is to study the effect of welding on the corrosion resistance of the austenitic stainless steel Alloy 59 (UNS N06027) as well as the galvanic corrosion generated by the base/weld pair estimated from the polarisation curves according to the mixed potential theory. The materials have been exposed to polluted phosphoric acid at several temperatures. The microstructure of the samples was studied by SEM and EDX analysis. The results show that the welding process shifts the corrosion potential values to more anodic potentials. The corrosion current densities and the passive current densities also increased by the effect of welding. This effect is aggravated with the increase in temperature. Open circuit potential values were located in the passive zone of the potentiodynamic curves, which means that the materials passivated spontaneously.The galvanic corrosion of the pair is not severe in the studied conditions. The ratio between the galvanic current density of the pair and the corrosion current density of the uncoupled anode is less than 5, which implies compatibility of the members in the couple.

1. INTRODUCTION

More than 95% of the phosphoric acid is obtained by the wet process (WPA). This process involves the attack of the phosphate rock by sulphuric acid followed by filtration of the pulp and the concentration of the acid. Therefore, severe corrosion problems may be caused by the presence of impurities such as chlorides, fluorides and sulphates in the hot phosphoric acid [1-6]. This is one of the

reasons why in the industrial manufacturing of phosphoric acid, stainless steels are present in all the units of production (digestion, filtration and concentration).

Austenitic stainless steels present good corrosion resistance in phosphoric acid media, due to their chromium, nickel and molybdenum content. The high chromium content of stainless steel leads to a great corrosion resistance due to the protective oxide layer formed on its surface [7, 8]. A high nickel content in these alloys increases pitting corrosion resistance [9, 10]. Additionally, molybdenum also improves the localised corrosion resistance of stainless steel, [11, 12].

Several types of these steels are used in welded structures (agitators, pumps, tanks, pipes) in the phosphoric acid industry. However, these materials are subjected to drastic conditions of corrosion due to the aggressive chemical acid [3-6] loaded with impurities (chlorides, sulphates…) contained in the ore, or introduced into the wash water with other thermal (temperature) and mechanical (abrasion) constraints [13-15].

Generally, a welded material is composed of three zones with different corrosion behaviours: base zone (BZ), heat-affected zone (HAZ) and weld zone (WZ). The heat affected zone next to the welding can be more likely attacked due to the metallurgical changes caused by heating cycles. It can become more sensitive to corrosion as a consequence of the precipitation of chromium carbides in the HAZ [16,17], which is of important concern in the technology of corrosion [18].

The welding process alters the microstructure of the materials, causing local variations in the composition and structure of the material. These changes increase the dissimilarity of the base/weld pair and can cause galvanic corrosion [19]. Previous works [20-23] has shown that corrosion is more severe in the contact region between the base and the welded zones. This is mainly due to the galvanic corrosion between the base and the welded metal.

Therefore, the goal of the present work is to study the effect of the welding process on the corrosion resistance of the UNS N06027 alloy (Alloy 59) and on the galvanic corrosion between Alloy 59 and the welded Alloy 59 in 40 wt. % phosphoric acid polluted with sulphuric acid and chloride ions at 20, 40, 60 and 80 ℃ using electrochemical measurements and microscopic techniques. The Energy dispersive X-ray analysis (EDX) was used to study the changes in the composition of the welded metal.

2. MATERIALS AND EXPERIMENTAL PROCEDURE

The tested material was an austenitic stainless steel UNS N06027 (Nicrofer S 5923hMo) provided by Krupp VDM (Germany) and denominated Alloy 59, which is classified in the range of high corrosion resistant alloys. This alloy is particularly suitable for applications in the chemical and petrochemical industries. The welding of Alloy 59 was carried out by the tungsten inert gas (TIG) process. The base material was used as a filler too. The chemical composition of the welded alloy is shown in Table 1.

Table 1. Chemical composition (wt %) of Alloy 59.

	Cr	Ni	Mo	Mn	Si	C	Fe	S	P
Alloy 59	23	60.75	15.6	0.15	0.02	0.006	0.29	0.003	0.002

For welding, a tungsten electrode in an argon atmosphere was used. The welding conditions were maintained constant for all the welded samples (current 50 A, voltage 26 V and argon flow 8 l/min). Once the welding was completed, the welded material was cut into three zones: base zone (BZ), heat-affected zone (HAZ) and weld zone (WZ). An area of 0.785 cm^2 was exposed to the solution.

In all the cases, the samples were wet abraded from 500 silicon carbide (SiC) grit to 4000 SiC grit, and were finally rinsed with distilled water. The tests were carried out in a three-electrode electrochemical cell. The potential of the working electrode was measured against a saturated calomel electrode (SCE) reference electrode. The auxiliary electrode was a platinum (Pt) wire. The electrolyte used in this study was the phosphoric acid (40 wt. %) with the addition of chemical impurities (4 wt. % of H_2SO_4 and 0.04 wt. % of chloride ions used as KCl). The corrosion behaviour of the alloy was analysed at different temperatures (20-80 °C). Temperature was controlled by regulating the heater power with a compatible control thermostat.

The materials were examined by optical microscopy and scanning electron microscopy (SEM) in order to estimate possible microstructural variations due to the TIG welding procedure. Energy Dispersive X-ray analysis (EDX) was adopted to determine the changes in the composition of the welded alloy.

The polarisation curves were carried out at a scan rate of 0.5 mV/s with a 263A potentiostat/galvanostat EG&G model. In all the cases, the tests were repeated at least three times and the scans presented in the paper are one of the obtained curves. Before each polarisation, the sample was immersed in the test solution for 1 h at the open circuit potential (OCP) [24]. After the OCP measurement, the specimen potential was reduced progressively to -600 mV$_{SCE}$ during 1 min in order to create reproducible initial conditions. Then, cyclic potentiodynamic curves were recorded from -600 mV$_{SCE}$ to 1200 mV$_{SCE}$. When the current density reached 10 mA/cm^2, the potential scan was reversed in order to evaluate the repassivation trend. Corrosion potential (E$_{corr}$) and corrosion current density (i$_{corr}$) were determined to obtain information about the general electrochemical behaviour of the materials. Besides, passivation current density (i$_p$) and breakdown potential (E$_b$) were also calculated.

The galvanic corrosion generated by the electrical contact between the base and the weld alloy was estimated from the polarisation curves according to the Mixed Potential Theory [25].

3. RESULTS AND DISCUSSION

3.1. Materials microstructure

The goal of the microstructural analysis was to evaluate the effect of welding on the microstructure of the welded Alloy 59 and to determine how these changes could affect the chemical

composition of various components. This study was conducted using the scanning electron microscope (SEM) coupled with the energy dispersive X-Ray (EDX).

Table 2. EDX analysis on the BZ, HAZ and on the WZ (wt %).

	BZ	HAZ	WZ	
			Dendrite cores	Grain boundaries
Cr	22.08	22.20	21.95	25.10
Ni	58.13	58.04	58.33	58.78
Mo	15.87	15.33	12.83	27.22
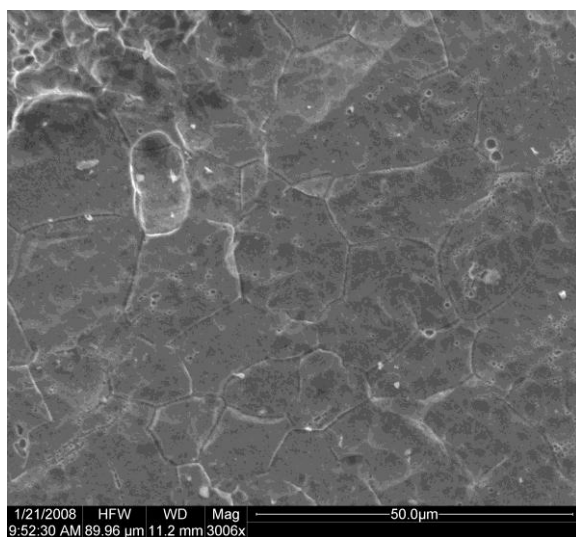
a. BZ
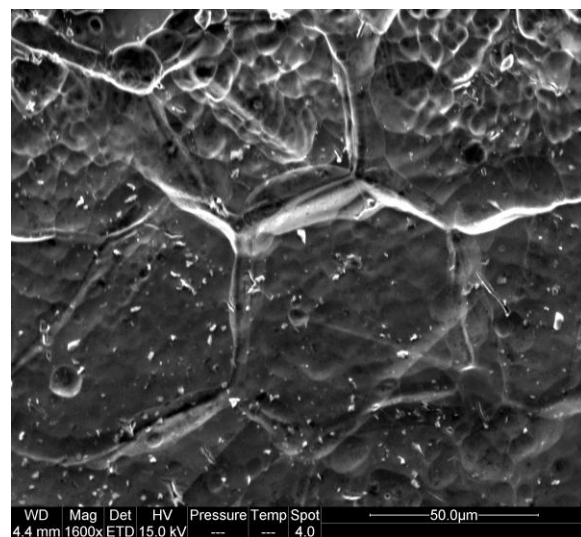
b. HAZ
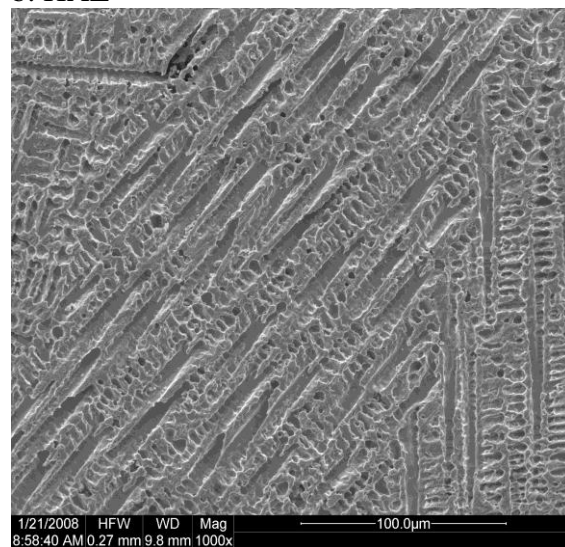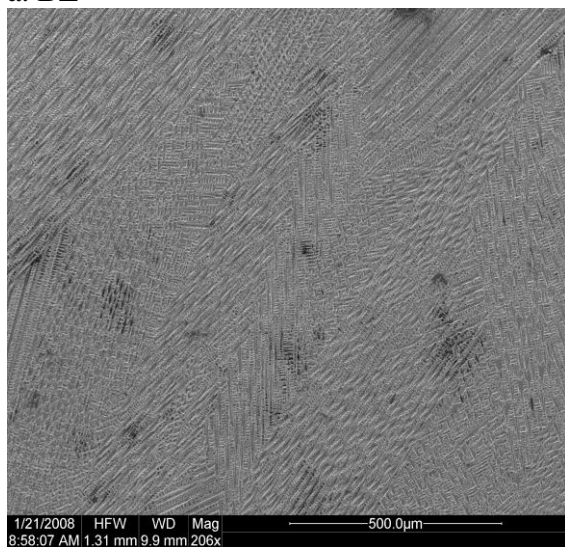
c. WZ

Figure 1. Microstructure of Alloy 59 in the different studied zones: **a.** BZ, **b.** HAZ and **c.** WZ

The base, the heat affected and the weld zones were chemically etched (1 volume HNO_3 at 65 wt. %, 2 volumes HCl at 36 wt. % and 1 volume H_2O).

Figure 1a shows the microstructure of the base zone. This is a single-phase austenite microstructure with equiaxed grains, typical microstructure of austenitic stainless steels.

The microstructure of the heat affected zone adjacent to the weld bead can be observed in Figure 1b. This zone is characterised by an increase in grain size due to the fact that, for stainless steels, there is no transformation point at temperatures higher than room temperature [26]. The weld zone exhibits an austenite microstructure of Windmanstätten (Figure 1c), characteristic of the solidification processes of metals [27]. The obtained microstructure is characterised by elongated key lines in a clear direction.

The Energy Dispersive X-ray analysis (EDX) shows a similar composition of HAZ and BZ with mean Cr values around 22 wt. %, Ni contents of 58 wt. % and Mo values around 15 wt% (Table 2). In the weld zone, the accumulations of chromium and molybdenum were detected in the grain boundaries. The content of Mo and Cr is higher in the grain boundaries than in the dendrite cores, as it can be seen in Table 2. This segregation of alloying elements during solidification leads to the depletion of Cr and Mo in the dendrite cores.

3.2. Potentiodynamic tests

3.2.1. Open circuit potential (OCP)

The open circuit potential (OCP) values for the three analysed specimens studied in the polluted phosphoric acid solution are shown in Table 3. They were calculated as the mean value of the last five minutes record [24]. BZ presents the most noble potential for all the studied temperatures. Moreover, in all the cases, the welding process shifts OCP to more active values compared with the base and the heat affected zones.

Table 3. Corrosion parameters of BZ, HAZ and WZ at different temperatures in a polluted phosphoric acid solution.

	Material	OCP (mV_{SCE})	E_{corr} (mV_{SCE})	i_{corr} ($\mu A/cm^2$)	i_p ($\mu A/cm^2$)	E_b (mV_{SCE})
20ºC	BZ	-20	-167	36	128	1135
	HAZ	-40	-183	51	192	1138
	WZ	-116	-213	84	194	1136
40ºC	BZ	-50	-178	50	196	1129
	HAZ	-84	-198	60	183	1127
	WZ	-129	-252	67	171	1080
60ºC	BZ	-83	-190	55	203	1127
	HAZ	-94	-208	101	224	1112
	WZ	-136	-260	110	265	1070
80ºC	BZ	-208	-217	119	218	1123
	HAZ	-226	-228	135	406	1044
	WZ	-238	-267	163	479	1058

For instance, working at 20 ºC, open circuit potential values were -20, -40, and -116 mV$_{SCE}$ for BZ, HAZ and WZ, respectively (Table 3). It can be seen that under the same temperature operating conditions, the base zone showed a more positive OCP value (more noble) than those of the heat affected and weld zones. This is due to the greater stability of the base metal surface in contact with the polluted acid solution. Also, it may be assumed that at a free potential, the formation of a stable and protective layer was spontaneous on the stainless steels surfaces. Other authors observed similar results with AISI 316L stainless steels in LiBr and H$_3$PO$_4$ solutions [28-30].

Moreover, no changes were observed on Alloy 59 surface after one hour of immersion at 80 °C (Figure 2), which confirms that the passive film formed on the surfaces of the three samples during immersion in the polluted phosphoric acid solution is resistant. This result indicates a good stability of the material/solution system even in the presence of impurities and under the most severe conditions of temperature. Concretely chromium oxide is considered the main passive component of the passive film in the anodic polarization of stainless steels. On the other hand, phosphoric acid media favour the formation of iron phosphates. Phosphate species can precipitate with dissolved iron species to form iron phosphates, since these compounds are characterised by a low solubility. Precipitation of iron phosphate occurs at the interface; that is:

$$6H_3PO_4 + 3Fe \;\; \rightarrow \;\; 3Fe(H_2PO_4)_2 + 3H_2$$

$$3Fe(H_2PO_4)_2 \;\; \rightarrow \;\; Fe_3(PO_4)_2 + 4H_3PO_4$$
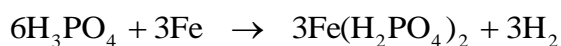
In phosphoric acid solutions, the passivation process is a combination of an inner chromium oxide layer together with an outer one formed with soluble Fe(H$_2$PO$_4$)$_2$ and the insoluble compounds FeHPO$_4$ and Fe$_3$(PO4)$_2$ [30].

Generally, OCP registers shifted towards more positive values with time, indicating good properties of the passive films formed on the surfaces of the alloys during the immersion in polluted phosphoric acid at the different studied temperatures. For all the cases, the WZ sample presents the most active OCP value (Table 3).

3.2.2. Potentiodynamic polarisation curves and electrochemical parameters

Figure 3 shows the effect of welding on the electrochemical behaviour of the three analysed materials (BZ, HAZ and WZ) in polluted phosphoric acid solutions at the different studied temperatures. For all the cases, no hysteresis loop is observed. The absence of hysteresis loop in all the tests is attributable to general corrosion processes. Therefore, it will not be possible to obtain the characteristic parameters of repassivation pitting.

Figure 2. Surfaces of BZ, HAZ and WZ of Alloy 59 after OCP tests in polluted phosphoric acid at 80 ºC.

a)

b)

c)

d)
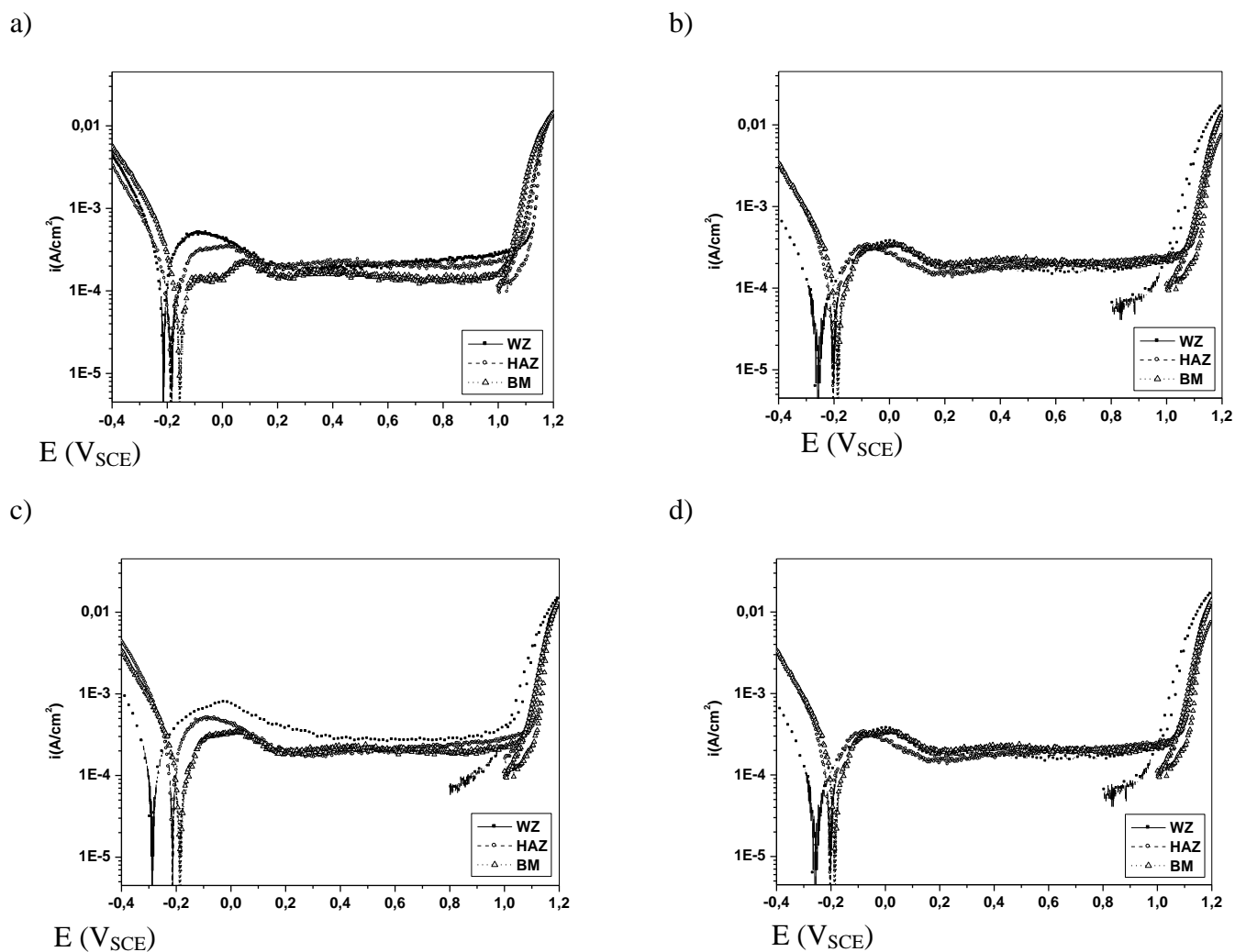
Figure 3. Potentiodynamic curves of the BZ, HAZ and WZ in polluted phosphoric acid solution at 20 ℃ (a), 40 ℃ (b), 60 ℃ (c) and 80 ℃ (d).

The polarisation curves of the BZ, HAZ and WZ show that the materials presented a typical curve of passivable alloys, since a passivity range was clearly observed at all the temperatures studied. This phenomenon might be explained by the formation of a protective oxide film during the test, which mainly consists of a layer of nickel and chromium oxide [21,31].

BZ registered a stable current density value over the whole passivity range. The HAZ presented an intermediate behaviour between the base metal and the weld zone. The WZ presented the same behaviour as that of BZ and HAZ. This material presented again a wide range of potentials within the passive zone at all studied temperatures, which can be attributed to the highest Mo and Ni content in its composition, since these elements are known to extend the passive layers on their surfaces.

The characteristic parameters of the corrosion resistance of the three different zones of the materials (BZ, HAZ and WZ) were obtained from Figure 3 and are shown in Table 3. Specifically, corrosion potential and corrosion current density values were obtained from the intersection of the Tafel line extrapolation of the potentiodynamic curves; that is, using the Tafel analysis for the different temperature.

Corrosion potentials (E_{corr}) shift towards more negative values by welding effect (Figure 3). The weld zone shows more active corrosion behaviour than BZ and HAZ at all the studied temperatures. The E_{corr} follows the same trend as the OCP values, although the latter are lower. This phenomenon is justified because during the open circuit measurements a protective oxide film was formed on the metal surface, shifting potential to more noble values. The OCP values obtained for the three analysed materials (BZ, HAZ and WZ) demonstrate that they passivate spontaneously since their values are situated on the passivity region of the polarisation curves (Figure 4). Moreover, in all the studied cases, the welding process shifts the OCP and the corrosion potential to more active values compared with the base material. These results are in good agreement with those found in a previous work [32].

The corrosion current densities (i_{corr}) obtained show that the highest values were obtained for the weld zone. At 20ºC, for example, the corrosion current density corresponding to the weld zone reached 84 μA/cm^2, a value which is more than two times higher than that obtained for BZ (36 μA/cm^2). This result may be attributed to the morphological changes of the weld zone of Alloy 59 that are described in the literature [33,34].

Passive current densities (i_p) were not lower than their corresponding corrosion current densities, however, the BZ, HAZ and WZ presented a stable passivity range in all the studied conditions. In general, BZ shows the lower i_p values and HAZ and WZ presented similar values.

The breakdown potentials (E_b) indicate the breakdown of the passive film and were determined when current density reached 100 $\Box$A/cm^2 [8]. The E_b values are very similar regardless of the studied zone and temperature.
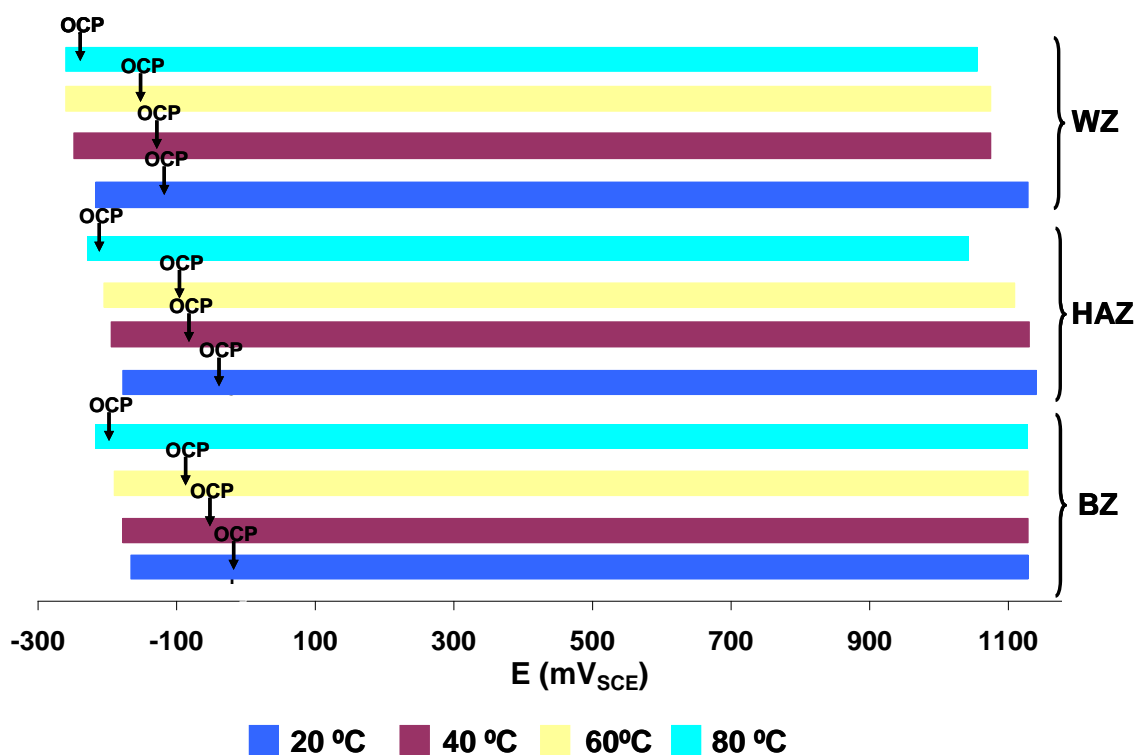
Figure 4. Situation of the OCP values on the passivity region of the polarization curves.

The difference between the breakdown potential and the corrosion potential (E_b-E_{corr}) was taken as an indicator of the range of potentials in which the alloy remains passive (passivity range).

Table 4. Passivity ranges of BZ, HAZ and WZ in polluted phosphoric acid at different temperatures.

Material	E_b-E_{corr} (mV)			
	20ºC	40ºC	60ºC	80ºC
Base Metal	1302	1307	1317	1340
HAZ	1321	1325	1320	1272
Weld Zone	1349	1322	1330	1325

Table 4 shows the passivity ranges of the three zones in the polluted phosphoric acid solution at the different temperatures. Additionally, Figure 4 shows the position of the OCP values in the passivation ranges. Table 4 and Figure 4 show similar passivity ranges for the different zones and analysed temperatures. However, WZ presents the widest passivity region.

In general, the weld zone presents the most negative corrosion potential and the highest passive current densities, so WZ will be more susceptible to corrosion, although the corrosion current densities did not follow a clear tendency with temperatures.

Previous works [20-23] have shown that the corrosion process is more severe in the contact region between the base and the weld zones in LiBr solutions. For a better understanding of the effect of the welding process action, the behaviour of the interfaces base/weld alloy will be analysed. That is, the galvanic corrosion between the base and the weld Alloy 59 will be studied.

3.2.3. Galvanic corrosion behaviour of Alloy 59 and welded Alloy 59

The direct measurement of galvanic couples provides information on the intensity of galvanic currents. However, to better understand the specific kinetic parameters of the galvanic cell, the mixed potential theory was selected.

Table 5. Couple potentials (E_{couple}), couple current densities (i_{couple}), difference E_{corr_c}-E_{corr-a} and ratio i_{couple}/i_{corr} at the different temperatures. Letters A and C refer to anodic and cathodic, respectively.

Temperature	Material	E_{corr} (mV$_{SCE}$)	E_{couple} (mV$_{SCE}$)	E_{corr_c}-E_{corr-a} (mV)	i_{couple} ($\mu A/cm^2$)	i_{couple}/i_{corr}
20 ºC	Welded metal (A)	-213	-188	56	180	2,15
	Base metal (C)	-157				
40 ºC	Welded metal (A)	-252	-204	64	104	1,55
	Base metal (C)	-188				
60 ºC	Welded metal (A)	-260	-232	70	280	2,53
	Base metal (C)	-190				
80 ºC	Welded metal (A)	-267	-234	50	201	1,23
	Base metal (C)	-217				

Galvanic corrosion of alloys treated by the application of the mixed potential theory was first described by Wagner and Traub [25]. The theory is based on two simple hypotheses: (1) any electrochemical reaction can be divided into two or more oxidation or reduction reactions, and (2) there can be no net accumulation of electrical charges during an electrochemical reaction. When two different corroding alloys are coupled electrically in the same electrolyte, both alloys are polarised so that each corrodes at a new rate [35].

The galvanic corrosion between Alloy 59 and the welded Alloy 59 pair was studied according to the Mixed Potential Theory [25]. The polarisation curves of Alloy 59 and the welded metal in semilogarithmic representation in region of E_{corr} are shown in Figure 5.

Table 5 summarises the corrosion potential (E_{corr}) of the uncoupled metals, as well as the mixed potential established between the pair (E_{couple}) and the differences between the corrosion potential of the cathodic and the anodic member of the pair (E_{corr_c}-E_{corr_a}). Aditionally, Table 5 shows the couple current density generated due to the coupling of the pair (i_{couple}) and the ratio i_{couple}/i_{corr}.

First of all, according to Table 5, for all the cases, the corrosion potential of the weld zone of Alloy 59 is more active than that of the base zone (Figure 5), indicating that the weld Alloy 59 is the anode of the pair at all the temperatures. This fact could be attributed to the segregation of the alloying elements during solidification, which diminishes the corrosion resistance of the weld zone. The corrosion resistance of the weld zone decreases due to the galvanic effect produced by coupling with the base metal, while Alloy 59 remains protected.

c)

d)
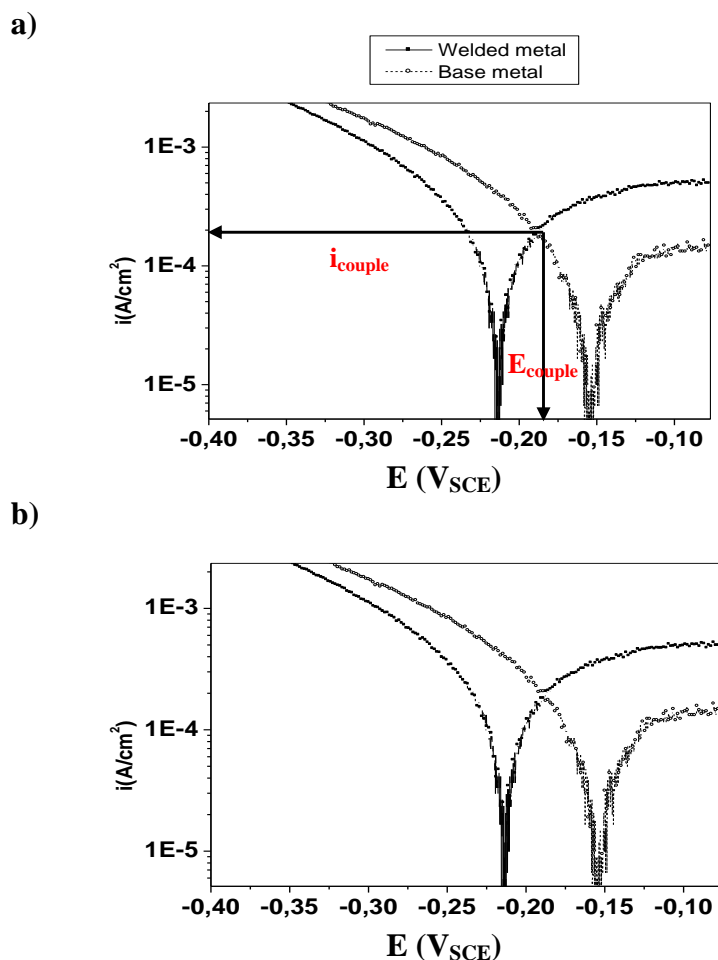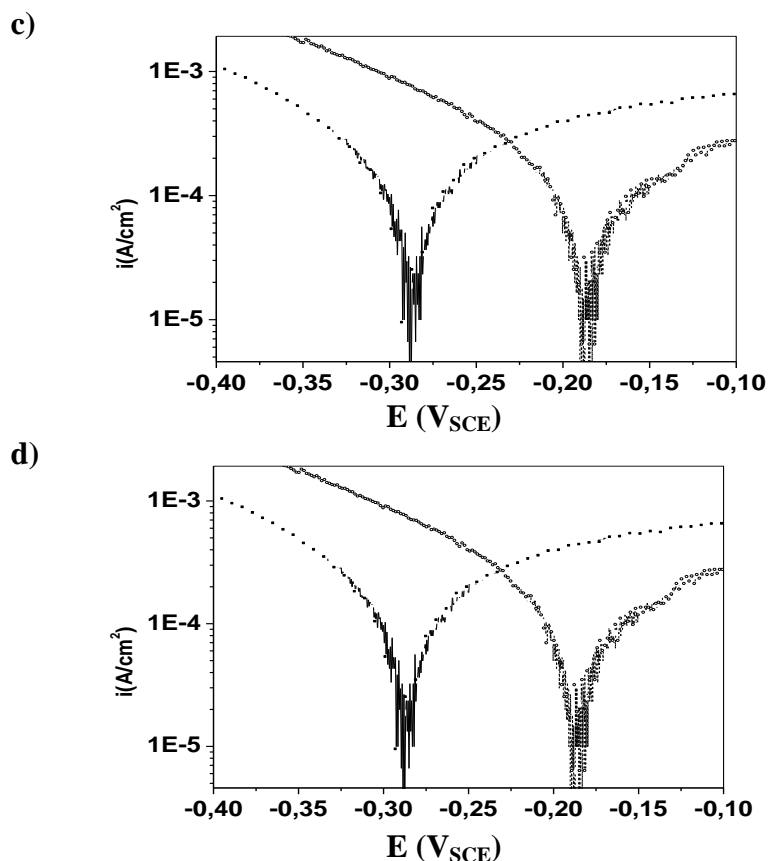
Figure 5. Superimposing of polarisation curves of the base and weld zones of Alloy 59 and in polluted phosphoric acid at 20 ºC (a), 40 ºC (b), 60 ºC (c) and 80 ºC (d).

The couple potential of the pairs shifted to more negative values as temperature increases, following the same trend observed in the corrosion potentials of each member of the pair. Besides, minimal differences of 100–130 mV between the corrosion potential of the cathode and the anode of the pair (E_{corr_c}-E_{corr-a}) are necessary to consider the galvanic effect significant [36]. In Table 5 it is possible to observe that, in spite of the fact that the weld zone was the anode at all the studied temperatures (from 20 to 80 ºC), the galvanic effect between the base and weld zones is hardly significant, with E_{corr_c}-E_{corr-a} values lower than 70 mV_{SCE}. Comparing Table 3 with Table 5 it can be observed that couple current densities are higher than the corresponding i_{corr} values of the weld zone (which is the anode of the pairs). This confirms that the weld zone increases its corrosion rate due to the galvanic coupling generated with the base zone.

According to Mansfeld and Kendel [37], the relative increase in the corrosion rate of the anode of the pair could be expressed by the ratio i_{couple}/i_{corr}, where i_{corr} is the corrosion current density of the uncoupled anode. The magnitude of this ratio may be used as a guide that reflects the severity of the galvanic effect in a couple, and it was suggested that a value less than 5 implies compatibility of the members of the pair [38]. The i_{couple}/i_{corr} values shown in Table 5 are, for all the cases, lower than 5, which implies compatibility of the members of the pair. Therefore, it could be concluded that the

galvanic corrosion between the base and weld Alloy 59 is not severe in polluted phosphoric acid solutions at the different studied temperatures.

4. CONCLUSIONS

Welding causes a variation in the composition (segregation of chromium and molybdenum) and microstructure (austenitic to dendritic microstructure) of Alloy 59. The OCP values obtained during the test indicate that the specimens (BZ, HAZ and WZ) spontaneously passivated in polluted phosphoric acid solutions at the different temperatures (20-80 ºC); this fact indicates their resistance to corrosion.

The electrochemical results show that the welding process shifts corrosion potential (E_{corr}) to more cathodic values. The corrosion and the passivation current densities increase as a consequence of welding, involving a decrease in corrosion resistance. This phenomenon is accentuated at higher temperatures. Moreover, the polarisation curves have shown the absence of hysteresis loop, a characteristic phenomenon of general corrosion processes in the tested medium.

Microstructure variations caused by welding convert the weld zone into the anode of the galvanic pair formed with the base zone of the materials; although the galvanic effect between base Alloy 59 and the weld zone is hardly significant in the studied conditions. It can be concluded that the galvanic corrosion between the base/weld pairs will not be severe working with polluted H_3PO_4. Consequently, Alloy 59 can be used as a structural material in the industrial equipment of phosphoric acid plants.

References

1. N. Bui, A. Irzo , F. Dabosi, A. Guenbour, A. Ben Bachir, *Ann. Chem. Fr.* 8 (1983) 411-422.
2. P. Decker, Phosphates and Phosphoric Acid, *Marcel Dekker Inc.,* New York, 1989.
3. A. Bellaouchou, A. Guenbour, A. Ben Bachir. *Corrosion* 49 (1993) 656-662.
4. A. Guenbour, S. Zeggaf, A. Ben Bachir, M.L. Escudero, M.F. Lopez. *Corrosion* 55 (1999) 6-11.
5. H. Iken, R. Basseguy , A. Guenbour , A. Ben Bachir, *Electrochimica Acta* 52 (2007) 2580-2587.
6. T. Poornima, Jagannath Nayak, A. Nityananda Shetty. *International Journal of Electrochemical Science* 5 (2010) 56-71.
7. T. Bellezze, G. Roventi, R. Fratesi, *Electrochimica Acta* 49 (2004) 3005–3014.
8. M. Kaneko, H.S. Isaacs. *Corrosion Science* 42 (2000) 67–78.
9. P.I. Marshall, T.G. Gooch. *Corrosion* 49 (1993) 514–526.
10. A.A. Hermas, K. Ogura, S. Takagi, T. Adachi. *Corrosion* 51 (1995) 3–10.
11. K. Sugimoto, Y. Sawada. *Corrosion Science* 17 (1977) 425–445.

12. K. Sugimoto, Y. Sawada. *Corrosion* 32 (1976) 347.
13. A. Guenbour, J. Faucheu, A. Ben Bachir, F. Dabosi, N. Bui. *Corrosion Journal* 23 (1988) 4.
14. A. Guenbour ,M.A Hajji ,E.M. Jallouli , A.Ben Bachir. *Applied Surface Science* 253 (2006*)* 2362-2366.
15. A. Bellaouchou, B. Kabkab, A. Guenbour, A. Ben Bachir. *Progress in Organic Coatings* 41 (2001) 127-132.
16. R. Leiva Garcia, M.J. Muñoz Portero, J. Garcia Antón. *International Journal of Electrochemical Science* 6 (2011) 442-460.
17. E. Folkhard. Welding metallurgy of stainless steels, Springer, Viena, (1988).
18. J.A. Brooks, A.W. Thompson, J. Williams, *Welding Journal* 34 (1984) 71s-83s.
19. T. Hemmingsten, H.Hovdan, P. Sanni, N.O.Aagotnes. *Electrochimica Acta* 47 (2002) 3949-3955.
20. E. Blasco-Tamarit, A. Igual-Munoz, J. Garcia-Anton, D. Garcia-Garcia. *Corrosion Science* 48 (2006) 863–886.
21. E. Blasco-Tamarit, A. Igual-Muñoz, J. Garcia-Anton. *Corrosion Science* 49 (2007) 4452.
22. E. Blasco-Tamarit, D.M. García-García, J. García-Antón. *Corrosion Science* 53 (2011) 784-795.
23. E. Blasco-Tamarit, A. Igual-Muñoz, J. Garcia-Anton, D.M. García-García. *Corrosion Science* 49 (2007) 1000-1026.
24. ASTM G5 - 94 (2004) Standard reference test method for making potentiostatic and potentiodynamic anodic polarization measurements.
25. C. Wagner, W. Traud. *Z Electrochem* 44 (1938) 391 454.
26. G. Conde y Santiago, Aceros inoxidables, refractarios y criogénicos, firsted. Interciencia, Madrid, 1971.
27. Metallography and Microstructures, American Society for Metals, (Eds.), spring, 1995.
28. R. Sánchez-Tovar, M.T. Montañés, J. García-Antón, *Corrosion Science* 52 (2010) 1508–1519.
29. R. Sánchez-Tovar, M.T. Montañés, J. García-Antón, A. Guenbour, A. Ben-Bachir, *Corrosion Science* 53 (2011) 1237–1246.
30. R. Sánchez-Tovar, M.T. Montañés, J. García-Antón, A. Guenbour. *International Journal of Electrochemical Science* 6 (2011) 3656-3670.
31. A. Neville, T. Hodgkiess, *Corrosion Science* 38 (1996) 927–956.
32. E.A. Abd El Meguid, A.A. Abd El Latif. *Corrosion Science* 49 (2007) 263–275.
33. W.E. White, *Mater. Charact.*1992; 28, p 349
34. M. Dadfar, M.H. Fathi, F. Karimzadeh, M.R. Dadfar, A. Saatchi, *Materials Letters* 61 (2007) 2343.
35. Baboian R. Electrochemical techniques for predicting galvanic corrosion. In: Baboian R, France Jr WD, Roew Lc, Rynewicz JF, editors. Galvanic and pitting corrosion field and Laboratory Studies. ASTM STP 576, Philadelphia: ASTM, 1976. p. 619.
36. E. Otero Huerta, Corrosion y Degradacion de Materiales, Sintesis, 1997.
37. F. Mansfeld, J. V. Kendel, Laboratory studies of galvanic corrosion of aluminium alloys, in: R. Raboian, W. D. France (Eds.), Galvanic and Potting Corrosion-Field and Laboratory Studies, ASTM STP 576, ASTM, 1976, pp. 20-47.
38. F. T. Cheng, K. H. Lo, H. C. Man, *Surface and Coatings Technology* 172 (2003) 316-321